SEMESTER THESIS

Automatic Analysis of Transmon Qubit Spectroscopy and Coil Coupling Measurements

Author:
Fadri Grünenfelder

Supervisor:
Johannes Heinsoo

ETH Zürich
Quantum Device Lab
Prof. Dr. Andreas Wallraff
September 16, 2016

Abstract

An already existing software suite has been extended by the functionality of determining the coupling of a transmon qubit's transition frequency to a coil or flux line via magnetic flux penetrating its SQUID loop. This coupling can be used to tune the qubit transition frequency in order to control the interaction with other qubits, resonators or drive lines. This thesis describes the implementation of functions which allow to perform automatic qubit and resonator spectroscopy and which find values of the magnetic coupling parameters. Automated characterization of qubits simplifies the scaling to higher number of qubits, which is a criterion for an universal quantum computer.

Contents

1 Introduction **3**

2 Superconducting Qubits **4**

2.1 The Cooper Pair Box 5

2.2 Transmon Qubit 7

2.3 Driving the Qubit 8

3 Coupling the Qubit to a Resonator **8**

3.1 Quantum Non-Demolition Readout 8

3.2 Qubit-Qubit Interaction 9

4 Four-Qubit Quantum Processor **9**

5 Software Suite **11**

6 Qubit and Resonator Spectroscopy **12**

6.1 Resonator Spectroscopy 12

6.2 Qubit Spectroscopy 14

6.3 Conclusion 15

7 Coupling to the Magnetic Field **16**

7.1 Determination of $\mathbf{k}_i$ via Fourier transform 16

7.2 Determination of $\mathbf{n}_i$ via parabola fit 17

7.3 Parameter Extraction 17

7.4 Voltages as Functions of the Qubit Transition Frequencies 19

7.5 Discussion 19

8 Adaptive Bayesian Experimental Design **19**

8.1 Discussion 22

9 Conclusion and Outlook **23**

10 Acknowledgements **24**

1 Introduction

The size of circuits in classical computers was subject to exponential decrease with time during the last decades [Schaller, 1997]. However, if the decrease in size still follows the same law in the future, then the size of the transistors inside a computer will soon reach the atomic length scale and therefore quantum effects will come into play. In classical computers, in which information is treated in units of bits, it is not clear how these quantum effects are to treat. However, there is an approach in information theory, called quantum information theory, which generalizes the concept of a bit to a qubit. Qubits are quantum mechanical two level systems. As all quantum systems, they can exist in superposition between different states. This means we can find our system in one of the classical states $|0\rangle$ or $|1\rangle$ but also in a superposition state $|\psi\rangle = \alpha\,|0\rangle + \beta\,|1\rangle$. When we measure this state $|\psi\rangle$, we end up in $|0\rangle$ with probability $|\alpha|^2$ and in $|1\rangle$ with probability $|\beta|^2$. This superposition states can be used to manipulate different states simultaneously. A NOT-gate for example maps $|0\rangle$ to $|1\rangle$ and vice versa. The quantum NOT-gate maps the state $|\psi\rangle$ to $\alpha\,|1\rangle + \beta\,|0\rangle$. This example can be gerneralized to an arbitrary function f which can be written in terms of gates and maps n bits to n bits. If we want to evaluate the function f at any possible argument, we create a superposition $|\psi_n\rangle = \alpha_1\,|00\ldots00\rangle + \alpha_2\,|00\ldots01\rangle + \cdots + \alpha_{2^n}\,|11\ldots11\rangle$. Then we take the circuit which represents f and let it act on $|\psi_n\rangle$. The resulting state is $\alpha_1\,|f(00\ldots00)\rangle + \alpha_2\,|f(00\ldots01)\rangle + \cdots + \alpha_{2^n}\,|f(11\ldots11)\rangle$, this means we have calculated all possible values of f by applying the gate only once. Unfortunately, the fundamental laws of quantum mechanics prevent us from reading out all the values at once. For some specific tasks however, quantum algorithms have been found that make use of evaluating a function at all its arguments, the most popular among them are the Deutsch-Josza [Deutsch and Jozsa, 1992], Grover [Grover, 1996] and Shor [Shor, 1997] algorithm. The Shor algorithm, for

example, is able to factor prime numbers in polynomial time, whereas the best known classical algorithm needs exponential time. An interesting question is whether it is possible or not to find such quantum mechanical two level systems and control them.

There are several approaches to realize quantum computers, such as trapped ions [Benhelm et al., 2008], NMR systems [Gershenfeld and Chuang, 1997], photons [Knill et al., 2001], Nitrogen vacancy centers in diamond [Neumann et al., 2010] or superconducting qubits [Clarke and Wilhelm, 2008]. This thesis focuses on a specific design of superconducting qubits called transmon qubits [Koch et al., 2007]. Single qubit gates, for example the above mentioned NOT gate, can be perfomed by applying microwave pulses to the qubit. To perform multiple qubit gates, the qubits need controlled interaction with each other. The qubit interact if they are in resonance with each other. Therefore we need a possibility to tune the qubits into resonance with each other in a controlled way. The transmon qubits can be tuned by applying an external magnetic flux through the circuitry representing the transmon qubit. After having built a qubit it is neccessary to characterize it such that precise control is possible.

The characterization is an important step towards precise control of a transmon qubit. The characterization itself is a time consuming process which has to be done for each new sample of a quantum processor. Additionally, the characterization consists of several tasks that are similar for a lot of different samples. Therefore it is desirable to have software which is able to perform the characterisation automatically. In this work, several characterisation tasks were automated, for example qubit spectroscopy to find the qubits current transition frequency. Another task that was automised is the determination of the coupling of the external magnetic flux to the Transmon qubit. Further, the developed software can, based on given frequencies, determine the experimental settings which tune the qubits to these frequencies.

The automatization of qubit characterization is a necessary task on the way to achieve a scalable quantum computer. Even for a small number of qubits, automated characterisation is faster than manually finding the qubits parameter values. The repetitive character of such characterisation tasks predestines them for automatization.

2 Superconducting Qubits

Superconducting circuits are macroscopic objects but show quantum effects [Nakamura et al., 1997], for example they possess quantized energy levels. We are interested in using these circuits for quantum information processing and therefore need an effective two level system. Quantizing one of the simplest electrical circuits, the LC oscillator, leads to an harmonic system, that means a system with infinitely many equally spaced energy levels [Baur, 2012]. One could now consider the first two energy levels as being the $|0\rangle$ and $|1\rangle$ states of a qubit. These two states are then called our computational subspace. However, because of the equal spacing of the energy levels this system is not a well-behaving qubit. This can be seen if we try to excite the system. We apply an electromagnetic pulse to excite the system from the ground state to the first excited state. During this process and because of the equal seperation of all the adjacent energy levels, we will unintentionally excite the system to a higher energy level. This would cause a loss of information due to the fact that the system is not any longer in our computational subspace. To prevent loss of information we need a

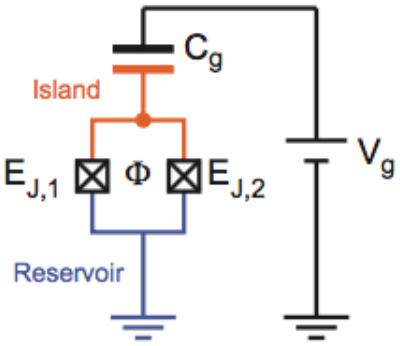

Figure 1: Circuit model of a CPB. The CPB consists of an island (orange), a reservoir (blue) and two Josephson junctions in parallel with energies $E_{\mathrm{J},1}$ and $E_{\mathrm{J},2}$ forming a SQUID loop. The loop is penetrated by a magnetic flux Φ. The SQUID loop is connected in series to a gate capacitor and the circuit is biased with a voltage V_{g}. Adapted from [Baur, 2012].

system with anharmonic level spacings.

2.1 The Cooper Pair Box

A Cooper Pair Box (CPB) is a superconducting circuit which consist of two parallel Josephson junctions which are together connected to a capacitor, as depicted in Figure 1. This circuit is then biased with a voltage V_{g}. The voltage bias allows us to control the number of Cooper pairs on the island. If we increase the voltage, Cooper pairs will tunnel from the reservoir to the island. The Josephson junction consists of two superconductors separated by a non-superconducting material [Josephson, 1962]. Together, these Josephson junctions form a so called SQUID loop (Superconducting Quantum Interference Device). This SQUID loop is very sensitive to magnetic flux [Zimmerman, 1977], which is used to tune the qubit frequency as we will see later.

The Hamiltonian of the CPB can be found by quantizing the circuit in Figure 1 [Bouchiat et al., 1998]. This Hamiltonian depends on the number of charges on the gate capacitor $n_{\mathrm{g}} = -C_{\mathrm{g}}V_{\mathrm{g}}/2e$, the Josephson energy $E_{\mathrm{J}}(\Phi) = E_{\mathrm{J}}^{\max}\,|\cos(\Phi/\Phi_0)|$ and the the charging energy $E_{\mathrm{C}} = e^2/2C_{\Sigma}$, where C_{Σ} is the total capacitance of the Cooper Pair Box. This Hamiltonian takes the form

$$\hat{H}_{\mathrm{CPB}} = 4E_{\mathrm{C}}(\hat{N} - n_{\mathrm{g}})^2 - E_{\mathrm{J}}\cos\hat{\delta} \tag{1}$$

expressend in terms of the number operator $\hat{N}$, which gives the number of charges on the island, and the phase operator $\hat{\delta}$ corresponding to the phase difference between the superconducting electrodes of the Josephson junction. The Josephson energy depends on the magnetic flux which penetrates

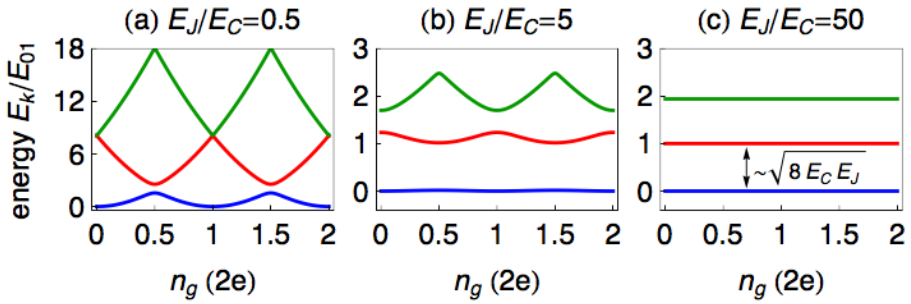

Figure 2: a) The first three energy levels of a Cooper Pair Box for $E_\mathrm{J}/E_\mathrm{C} = 0.5$ The blue curve is the ground state, the red one the first and the green one the second excited state. b) Shows the same three states but for $E_\mathrm{J}/E_\mathrm{C} = 5$. c) Shows the same three states for $E_\mathrm{J}/E_\mathrm{C} = 50$. Adapted from [Baur, 2012].

the SQUID loop. This depenency allows us to control the magnitude of the transition frequency by generating a magnetic field near the CPB. Experimentally this can be done by using coils or so called flux lines. A flux line is a conducting line on the quantum processor which passes by the qubit. When a voltage is applied to the flux line, it generates a magnetic field. This magnetic field is created for the purpose of tuning the transition frequency of the qubit. The same functionality can be achieved by mounting coils near the quantum processor. In contrast to the coils, the flux lines affect one qubit strongly and the other qubits weakly. In the following, most of the time only coils are mentioned, for example, we call the relation between the qubit transition frequency and the coils or flux lines qubit-coil coupling, but physically the coupling can be realized by using both coils or flux lines.

The Schrödinger equation in terms of the phase difference δ follows directly from the Hamiltonian if we use that the number operator and the phase operator are canonical conjugate variables. The Schrödinger equation is given by

$$E_k\psi(\delta) = \left[4E_\mathrm{C}\left(-i\frac{\partial}{\partial\delta} - n_\mathrm{g}\right)^2 - E_\mathrm{J}(\Phi)\cos\delta\right]\psi(\delta). \tag{2}$$

The solutions E_k of Equation 2 are the Mathieu functions [Cottet et al., 2002]. These solutions are shown in Figure 2 for $k = 0, 1, 2$ and for different ratios of Josephson energy and charging energy. The computational states $|0\rangle$ and $|1\rangle$ are the ground and the first excited state of the CPB and the Hamiltonian takes the form

$$\hat{H} = -\frac{1}{2}\hbar\omega_{01}\hat{\sigma}_z \tag{3}$$

in the computational basis. The transition frequency is $\omega_{01} = (E_1 - E_0)/\hbar$.

As we can see in Figure 2a, the slope of the eigenenergy changes if we vary n_g. This behaviour has a negative effect on the phase coherence. This issue becomes apparent when we look at the time evolution of a superposition of ground and first excited state. They evolve like

$$e^{-iE_0t/\hbar}\,|0\rangle + e^{-iE_1t/\hbar}\,|1\rangle = e^{-iE_0t/\hbar}(|0\rangle + e^{-i(E_1-E_0)t/\hbar}\,|1\rangle \tag{4}$$

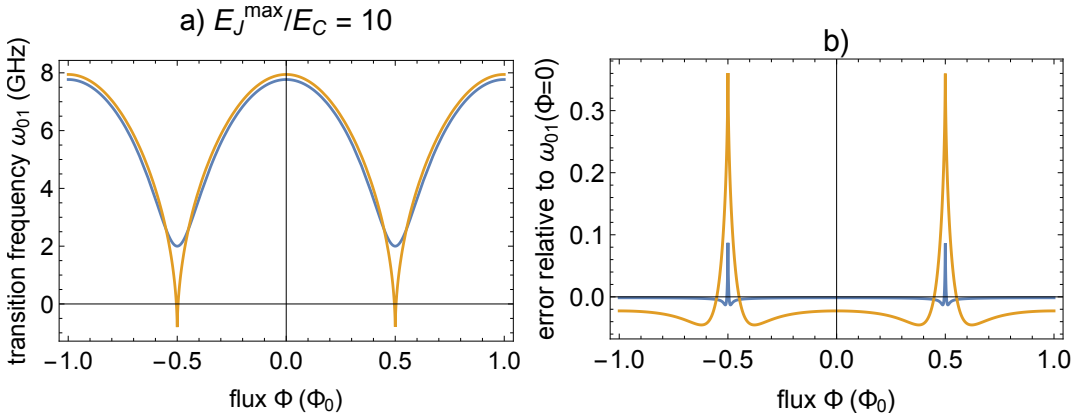

Figure 3: a) Exact (blue) and approximated (orange) solution for the transition frequency of the CPB with ratio $E_{\mathrm{J}}^{\mathrm{max}}/E_{\mathrm{C}} = 10$. b) Error $(\omega_{01}^{\mathrm{exact}}(\Phi) - \omega_{01}^{\mathrm{approx}}(\Phi))/\omega_{01}^{\mathrm{exact}}(0)$ relative to the exact maximum transition frequency for $E_{\mathrm{J}}^{\mathrm{max}}/E_{\mathrm{C}} = 10$ (orange) and $E_{\mathrm{J}}^{\mathrm{max}}/E_{\mathrm{C}} = 100$ (blue).

and if we have fluctuations in the charge on the capacitor, then the relative phase between the ground and first excited state fluctuates too. Therefore we are interested in a transition frequency which is approximately constant when varying the charge on the capacitor.

2.2 Transmon Qubit

We have seen that the sensitivity to charge noise is a big downside of the CPB. This issue can be resolved by going to the transmon limit, that means building the qubit such that $E_{\mathrm{J}}/E_{\mathrm{C}} \gg 1$. In Figure 2 the effects of increasing this ratio is shown. We can see that the slope of the energy dispersion becomes approximatively flat for large enough $E_{\mathrm{J}}/E_{\mathrm{C}}$. An established way to get a high ratio is to shunt a large capacitance to the Josephson junctions [Baur, 2012]. The tradeoff for the lower charge noise sensitivity is a smaller anharmonicity of the energy levels.

In the transmon limit, the Mathieu functions can be approximated with a simple analytical expression for the transition frequency between the ground and the first excited state [Koch et al., 2007]. The transition frequency then takes the form

$$E_{01} \approx \sqrt{8E_{\mathrm{C}}E_{\mathrm{J}}^{\mathrm{max}}|\cos(\pi\Phi/\Phi_0)|} - E_{\mathrm{C}}. \tag{5}$$

In Figure 3b the difference between the exact and approximated solution relative to the exact maximal transition frequency is shown. The error of the approximation increases with increasing $E_{\mathrm{J}}/E_{\mathrm{C}}$ ratio. For the case $E_{\mathrm{J}}/E_{\mathrm{C}} = 100$ only in a narrow region around the minimal transition frequency a significant error is present. Therefore it is reasonable to use the approximation in Equation 5.

2.3 Driving the Qubit

To drive the qubit we apply an AC gate voltage $V_{\mathrm{g}}(t) = V_{\mathrm{D}} \cos(\omega_{\mathrm{D}} t)$ (see Figure 2). This voltage leads to an additional term in the Hamiltonian [Baur, 2012]. The total Hamiltonian is of the form

$$\hat{H} \approx \frac{1}{2}\hbar\omega_{01}\hat{\sigma}_z + \hbar\Omega\cos(\omega_{\mathrm{D}} t)\hat{\sigma}_x \tag{6}$$

for small driving strength, where $\Omega = 4E_{\mathrm{C}}C_{\mathrm{g}}V_{\mathrm{D}}\sin\theta/e\hbar$ and $\theta = \arctan(\frac{E_{\mathrm{J}}}{4E_{\mathrm{C}}(1-2n_{\mathrm{g}})})$. Together with the free time evolution we can perform arbitrary single qubit operations.

3 Coupling the Qubit to a Resonator

The design of a transmon qubit was described in the previous section. However, to get a fully functional system for information processing, we need a way to read out the qubit state and to let qubits interact with each other. The readout can be performed by turning on a small interaction between the qubit and the environment. In the case of superconducting qubits this is achived by coupling the qubit to a transmission line resonator [Wallraff et al., 2004]. This field is referred to as circuit quantum electrodynamics (circuit QED).

3.1 Quantum Non-Demolition Readout

The coupled system consisting of the transmon qubit and the transmission line resonator can be operated in different regimes [Koch et al., 2007]. In this thesis only the dispersive regime is discussed. The frequency of the i-th transmon energy level is denoted with ω_i and the transition frequency from the i-th to the j-th level is $\omega_{i,j} = \omega_i - \omega_j$. The dispersive limit is reached when the detunings $\Delta_i = \omega_{i,i+1} - \omega_r$ between the transmon energy levels and the resonant frequency ω_r of the transmission line are large. This means that the coupling strength g_{01} between the resonator and the first transition frequency is much smaller than the detunings $g_{01} \ll |\Delta_0|, |\Delta_1|$. In a two level approximation we get the Hamiltonian [Koch et al., 2007]

$$\hat{H}_{\mathrm{disp}} = \frac{1}{2}\hbar\left(\omega_{01} + \frac{g_{01}^2}{\Delta_0}\right)\hat{\sigma}_z + \hbar(\tilde{\omega}_r + \chi\hat{\sigma}_z)\hat{a}^\dagger\hat{a}, \tag{7}$$

where

$$\chi \approx \frac{g_{01}^2 E_{\mathrm{C}}}{\Delta_0(\Delta_0 - E_{\mathrm{C}})} \tag{8}$$

in the transmon limit. The resonator frequency is also shifted according to the relation

$$\tilde{\omega}_r = \omega_r - \frac{g_{12}^2}{2(\omega_{12} - \omega_r)}. \tag{9}$$

The operators $\hat{a}^\dagger$ and $\hat{a}$ are the creation and annihilation operators of the photon mode inside the transmission line resonators.

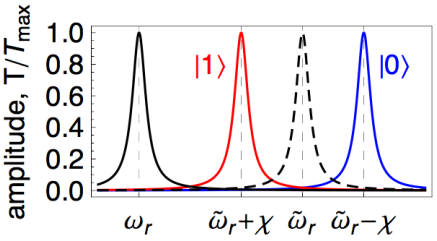

Figure 4: Amplitude of the resonator transmission spectrum for the uncoupled resonator (solid black lines), for the uncoupled resonator but with shifted frequency (dashed black lines), for the coupled resonator with the qubit in the ground state (blue line) and in the excited state (red line). Adapted from [Baur, 2012].

In Equation 7 we can see that the resonator frequency shifts depending on the state of the qubit. This fact can be used to determine the qubit frequency as described later in Subsection 6.2. The resonator frequency does not only depend on the state of the qubit, but also on the value of the transition frequency of the qubit. A change in the qubit transition frequency modifies χ and therefore changes the resonator frequency.

3.2 Qubit-Qubit Interaction

The interaction between two qubits can be achieved by coupling them to the same resonator [Blais et al., 2004]. If both qubits are tuned into resonance with each other and are in the dispersive regime with the resonator, the Hamiltonian describing the system is

$$\hat{H}_{2q} = \frac{1}{2}\hbar\left(\omega_{01} + \frac{g_{01}^2}{\Delta_0}\right)(\hat{\sigma}_z^1 + \hat{\sigma}_z^2) + \hbar[\tilde{\omega}_r + \chi(\hat{\sigma}_z^1 + \hat{\sigma}_z^2)]\hat{a}^\dagger\hat{a} + \hbar\frac{g_{01}^2}{\Delta_0}(\sigma_+^1\sigma_-^2 + \sigma_-^1\sigma_+^2), \tag{10}$$

where the operators σ_z^i and $\sigma_\pm^i$ act on qubit i. The evolution of the qubits corresponding to this Hamiltonian in the frame rotating with ω_{01} is

$$U_{2q}(t) = \begin{pmatrix} 1 & & & \\ & \cos\left(\frac{g_{01}^2}{\Delta}t\right) & i\sin\left(\frac{g_{01}^2}{\Delta}t\right) & \\ & i\sin\left(\frac{g_{01}^2}{\Delta}t\right) & \cos\left(\frac{g_{01}^2}{\Delta}t\right) & \\ & & & 1 \end{pmatrix}. \tag{11}$$

For $t = \pi\Delta/4g_{01}^2$ we get an $\sqrt{i\text{SWAP}}$ gate which forms together with single qubit operations an universal set of gates.

4 Four-Qubit Quantum Processor

One of the essential building blocks of classical and quantum computers is the processor. An established description of the desired properties of a quantum processor is given by the DiVincenzo

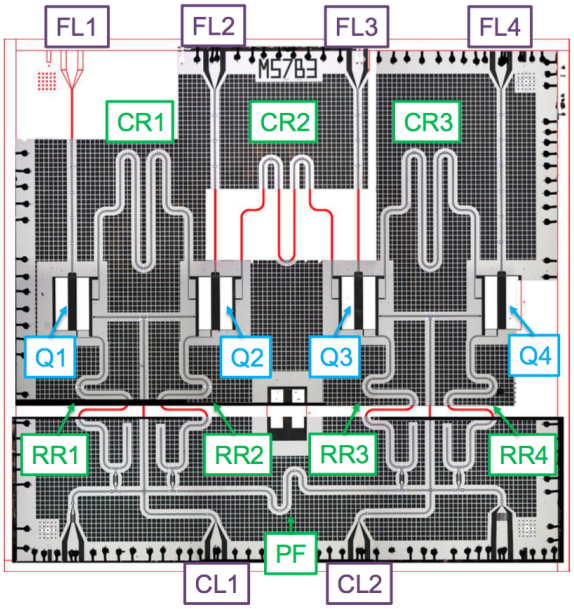

Figure 5: Sample used during this thesis. The qubits are labeled as QB1 - QB4, FL1 - FL4 are the flux lines , RR1 - RR4 are the readout resonators, CR1 - CR3 are the coupling resonators, PF is the Purcell filter and CL1 and CL2 are the charge lines. Image courtesy of Yves Salathé.

criteria [DiVincenzo, 2000]. DiVincenco proposed that a quantum computer primarily needs a scalable physical system with well characterized qubits. In this context, scalable means that we can include more qubits without changing the architecture of the processor. This condition can be met by the transmon qubits which are interconnected via resonators in a clever way. Further, DiVincenzo demands the ability to perfom an universial set of quantum gates. A set of gates is called universal if an arbitrary operation can be achieved by combining operations from this set. Such a set is given by single qubit operations which allow to generate an arbitrary state $\alpha\left|0\right\rangle+\beta\left|1\right\rangle$ starting from $\left|0\right\rangle$ and an entangling two-qubit interaction, for example a CNOT gate or the discussed $\sqrt{i\text{SWAP}}$ gate [Bremner et al., 2002]. A third criteria is the ability to read out the qubit state. A way to do this is to use multiplexed readout [Chen et al., 2012]. The multiplexed readout is a method which is compatible with the scalability requirement. There are two other criteria proposed by DiVincenzo regarding the coherence time and the initialization of the qubit.

The quantum processor which was used during this thesis includes 4 qubits as shown on the optical microscope photo of the sample in Figure 5. The flux lines are used to tune the qubit transition frequencies. The qubits are connected together with the coupling resonators. This coupling generates the interaction Hamiltonian in Equation 10 which allows us to perform two qubit gates on the coupled qubits. Single qubit gates can be performed by using the charge lines.

The sample possesses four readout resonators which are coupled to a common Purcell filter. This configuration allows multiplexed readout [Chen et al., 2012], which has the advantage that we need only one readout circuit to measure the state of all qubits.

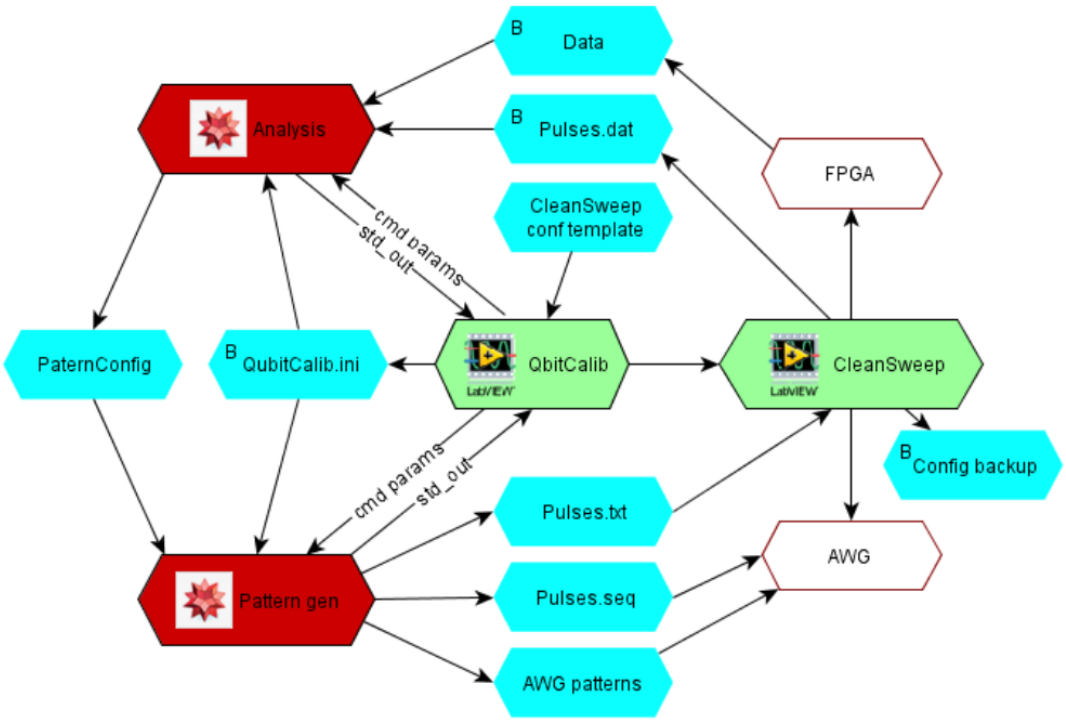

Figure 6: Software Suite and data flow. Mathematica scripts are colored in red, Labview scripts in green and files in blue. Adapted from [Heinsoo, 2013].

5 Software Suite

The experiment control software is a framework of *Wolfram Mathematica* and *LabView* scripts and VI's. A detailed description can be found in [Heinsoo, 2013, Ciorciaro, 2015]. The main LabView components are QubitCalib and CleanSweep, see Figure 6. CleanSweep communicates with the physical devices and QubitCalib performs automated calibration tasks. The file `QubitCalib.ini` contains rather abstract parameters like paths to other configuration files and paths for data in- and output and `PatternConfig` contains the parameters to generate pulses, e.g. puls length. The `Pulses` files contain the information about already generated pulses. In the file `AWG patterns` the waveforms, which are executed by the Arbitrary Wave Generators (AWGs), are stored. The *Wolfram Mathematica* scripts are used to perform the analysis of the measurements and for pattern gerneration for the next experiments.

The aim of the software suite is to allow us to perform advanced experiments which use complicated pulse sequences and to save time by automating characterization and experiments. Until now, new quantum processor samples had to be characterized manually, although the characterization procedure consists of similar steps for different samples. As an example, determining the relation between qubit transition frequency and magnetic flux, see Equation 5, consists of the same steps

independent of the sample. First, we have to measure the qubit transition frequency for different magnetic fluxes and then we determine the free parameters of the model describing this relation. In the past, these two steps were performed manually by sweeping each coil or flux line voltage separately. However, it would be much more time-efficient if we could use unsturctured data containing the transition frequency and the corresponding voltages on the coils or flux lines. This procedure is more time-efficient for the reason that we can use already existing data and we do not have to generate data especially for the purpose of finding this coupling. In the past, the qubit transition frequency was determined by analyzing the resonators transmission spectra by eye to find the resonances corresponding to the qubit frequency. This is another task which is time consuming when perfomed manually and it is tidious in the case we want to do it many times. Because knowing the qubit transition frequency is a basic tool to perform quantum information processing, it is inevitable to automatize it to allow scalability of the system. During this work these two tasks of performing qubit spectroscopy and determining the qubit-coil coupling were automated.

In Subsection 3.1 we have seen that the resonant frequency of the readout resonator shifts with the qubit transition frequency. In order to perfom qubit spectoscopy, as described later in section 6, we need to know the resonant frequency of the readout resonator. Therefore finding the qubit transition frequency consists of two parts. First, we have to find the resonant frequency of the resonator and then we can perform the qubit spectroscopy. Part of this work was to implement *Wolfram Mathematica* functions to perform this tasks automatically and to determine the qubit-coil coupling. The embedding of these functions into the software framework is part of an ongoing Master thesis [Storz, 2016].

6 Qubit and Resonator Spectroscopy

The precise manipulation of a qubit is only possible if we have detailed knowledge about the parameters of the qubit. One of the most important parameters is the qubit transition frequency, because only if we know the qubit transition frequency we can perform gates on the corresponding qubit. In this chapter we discuss a method to find the qubit transition frequency via an automated procedure.

As we have seen in section 3, we get different transmission amplitudes of the resonator depending on the qubit state and transition frequency. To find the qubit transition frequency ω_{01} we need to know the resonator's spectrum. Therefore, we first discuss the resonator spectroscopy and afterwards the qubit spectroscopy.

6.1 Resonator Spectroscopy

On the sample we have four readout resonators, each of them coupled to a qubit. These resonators are then coupled to a single Purcell filter to allow multiplexed readout as described in section 4. Our goal is now to find the spectrum of this coupled system.

The transmitted amplitude of the readout resonator coupled to the Purcell filter can be modeled by two driven coupled harmonic oscillators. However, such a model would possess six degrees of freedom, namely the amplitude, the decay rate and the resonance frequency for the readout resonator

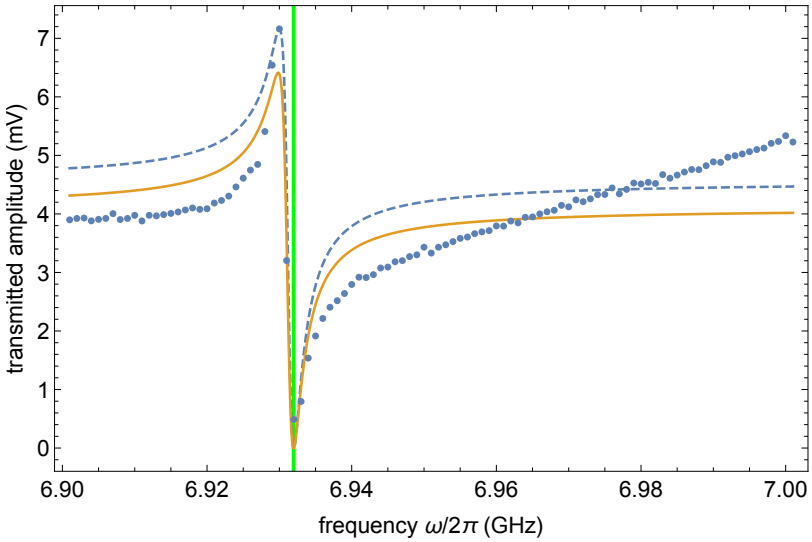

Figure 7: Transmitted amplitude of the Purcell filter coupled to the readout resonator of qubit 1. The blue dots represent the measured data, the blue dashed line shows the model function with guess values for free parameters and the orange solid line shows the fit. The green solid line indicates the frequency used to drive the Purcell filter for the subsequent qubit spectroscopy.

and for the Purcell filter. To reduce the complexity, we use here the Fano resonance, which has only three degrees of freedom. Approximating driven coupled harmonic oscillators by the Fano resonance is reasonable if one of the two oscillators possesses a much larger decay rate than the other. In our case, the decay rate of the Purcell filter is larger than the decay rate of the readout resonator. The model has the form

$$A(\omega) = A_r \frac{(q\Gamma_r/2 + \omega - \omega_r)^2}{(\Gamma_r/2)^2 + (\omega - \omega_r)^2}, \tag{12}$$

where properties of the readout resonator are labeled with r. These properties are the decay rate Γ_r, the amplitude A_r and the resonant frequency ω_r. The properties of the Purcell filter determine the value of the parameter q. We only fit the amplitude because we do not have phase information recorded, as we did not have phase reference in the measurement.

The parameters describing the measured data best were found by minimizing residuals from theoretical model to the measured transmitted amplitude of the Purcell filter coupled to the readout resonator. The spectroscopy result is shown in Figure 7. The Purcell filter determines the background. The peak and dip indicate the position of the readout resonators resonant frequency.

The resonator spectroscopy should be fully automated, therefore we need to calculate the guess values from the measured data, depicted in Figure 7 as blue points, via an algorithmic procedure. The guess for A_r is the mean of the transmitted amplitude with the highest frequency and the one with the lowest frequency in the measured data set. Analyzing the extrema of the model gives us

the frequencies $\omega_{\max}$ and $\omega_{\min}$ of the maximal and minimal transmitted amplitudes. They are

$$\omega_{\max} = \frac{\Gamma_r/2}{q} + \omega_r \tag{13}$$

$$\omega_{\min} = \omega_r - q\Gamma_r/2. \tag{14}$$

Inserting the maximum into the model gives us the equation

$$A_{\max} := A(\omega_{\max}) = \frac{(q + 1/q)^2}{1 + 1/q} \tag{15}$$

which allows us to guess q. Further we can guess Γ_r and ω_r via

$$\Gamma_r = 2\frac{\omega_{\max} - \omega_{\min}}{q + 1/q} \tag{16}$$

$$\omega_r = \omega_{\min} + q\Gamma_r/2. \tag{17}$$

The resulting parameters do not describe the experimental data with high accuracy. But for the purpose of performing a subsequent qubit spectroscopy we are only interested in the drive frequency with minimal amplitude. The result depicted in Figure 7 allows us to extract this frequency with a sufficient accuracy for the qubit spectroscopy.

6.2 Qubit Spectroscopy

In order to find the qubit frequency, we first have to find the resonator frequency which is also shifted when we tune the qubit, as discussed in section 3. We start by performing a resonator spectroscopy. Then the resonator is driven with a frequency which has a large difference in transmitted amplitude compared to the nearby frequencies. In the case of the resonator spectrum in Figure 7 we would choose the drive frequency marked by the green line. The algorithm which performs the qubit spectroscopy always chooses the frequency with minimal transmitted amplitude. The minimal transmitted amplitude is chosen because it is more distinctive than the maximum in the most cases and therefore numerically easier to find.

For the qubit spectroscopy itself we drive the resonator with the previously determined frequency. The qubit is driven through the local drive line, as described in Subsection 2.3. The drive frequency of the qubit is swept over a large range. When the qubit drive frequency hits the transition frequency of the qubit, the qubit gets excited. This leads to a shift in the readout resonator frequency, and therefore the transmitted amplitude through the resonator changes. We initially set the resonator to a frequency with minimal transmission and thus the transmitted amplitude increases when the qubit is excited. This leads to a peak in the transmitted amplitude of the readout line as a function of the qubit drive frequency, as shown in Figure 8. This peak gives us the transition frequency of the qubit, indicated by the vertical red line. If we drive the qubit with too high power, we will also drive the $0 \leftrightarrow 2$ transition. In Figure 8b we see two peaks, one is form the $0 \leftrightarrow 1$ transition and the other from the $0 \leftrightarrow 2$ transition. Because two photons were absorbed at the $0 \leftrightarrow 2$ transition, we see the peak at the frequency $\omega_{02}/2$.

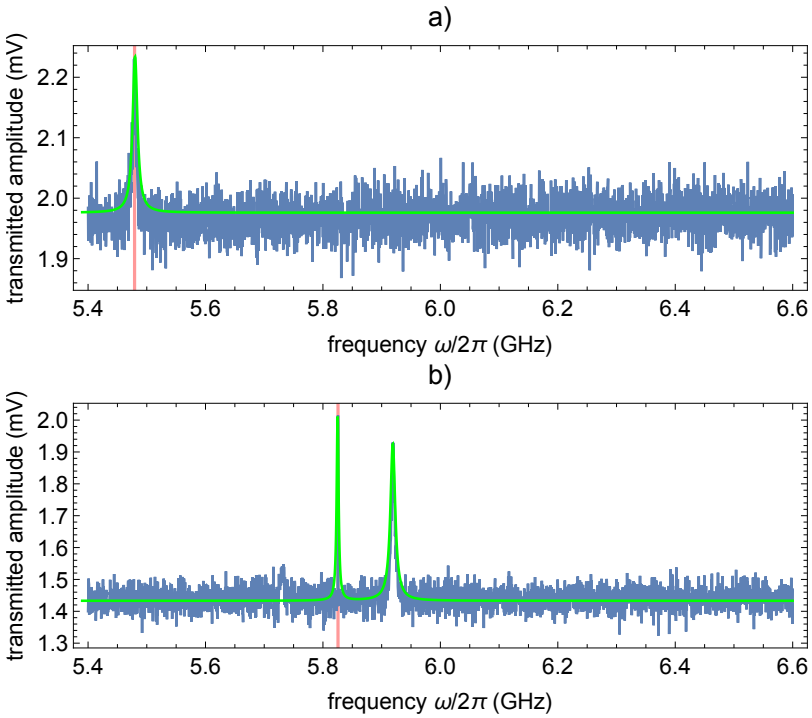

Figure 8: Transmitted amplitude of the readout line coupled to the resonator of qubit 1 while the frequency of the qubit drive is swept. The measured data is shown in blue, the model function in green. The numerically determined qubit frequency is indicated by the vertical red line. a) Spectroscopy for coil voltages $(V_1,V_2) = (9.9\,\mathrm{V}, 5.8\,\mathrm{V})$. b) Spectroscopy for coil voltages $(V_1,V_2) = (8.4\,\mathrm{V}, -5.4\,\mathrm{V})$. A second peak is visible in this spectrum due to excitation of the qubit's second energy level.

6.3 Conclusion

In this section we presented a way to automatically determine the qubit frequency. We started by performing a resonator spectroscopy. From the resonator spectrum we determined the resonator drive frequency. This frequency is then used to perform a qubit spectroscopy from which we could determine the qubit frequency. The knowledge of the qubit transition frequency is neccessary to be able to accurately tune the qubit. Only when we are capable of finding the qubit frequency we are able to perform quantum gates and therefore processing quantum information. Furthermore accurate automated qubit spectroscopy is a fundamental building block if we want to automatize more complicated tasks, for example finding the coupling of the qubit to a magnetic field or preparing the qubits in a Bell state.

7 Coupling to the Magnetic Field

Sending pulsed magnetic fields through the qubit's SQUID-loop is a tool that is used to perform two qubit gates [DiCarlo et al., 2009]. To use this tool in experiments, the qubit-coil/flux line coupling has to be known. In this section I would like to present an automated way to determine the coupling of the qubit to coils or flux lines. This coupling is mediated by the magnetic flux generated by coils or flux lines. The flux acts on the transition frecuency via the SQUID loop. In general we consider a sample with n_q qubits and n_c coils or flux lines. We can apply a voltage to all of the coils or flux lines. We can describe the voltage settings for the coils as a vector $\mathbf{V} = (V_1, V_2, \dots, V_{n_c})^\top$ and the flux penetrating the SQUID loops can be written as $\mathbf{\Phi} = (\Phi_1, \Phi_2, \dots, \Phi_{n_q})^\top$. The flux through the SQUID loop depends linearly on the voltages $\mathbf{V}$. We can write this relation in the form

$$\Phi_i = \mathbf{k}_i \cdot \mathbf{V} + \Phi_{\mathrm{env},i} \tag{18}$$

or

$$\mathbf{\Phi} = M \cdot \mathbf{V} + \mathbf{\Phi}_{\mathrm{env}}, \tag{19}$$

where $i \in 1, 2 \dots, n_q$. The additional term $\mathbf{\Phi}_{\mathrm{env}} = (\Phi_{\mathrm{env},1}, \Phi_{\mathrm{env},2}, \dots, \Phi_{\mathrm{env},n_c})^\top$ is a flux offset caused by the environment and the vectors $\mathbf{k}_i$ contain the geometric properties that relate the fluxes through the SQUID loops to the coil or flux line voltages. The i-th row of the matrix M is the vector $\mathbf{k}_i$. We define the vector $\boldsymbol{\omega}_{01} = (\omega_{01,1}, \omega_{01,2}, \dots, \omega_{01,n_q})^\top$ which contains the transition frequencies of all qubits. Then we insert Equation 18 into Equation 5 and get

$$\hbar\omega_{01,i} \approx \sqrt{8E_\mathrm{C}E_\mathrm{J}^{\max}\left|\cos\left(\pi\frac{\mathbf{k}_i \cdot \mathbf{V} + \Phi_{\mathrm{env},i}}{\Phi_0}\right)\right|} - E_\mathrm{C}. \tag{20}$$

The goal is to determine the parameters $E_\mathrm{J}^{\max}$, $\mathbf{k}_i$ and $\mathbf{\Phi}_{\mathrm{env}}$. The remaining parameter E_C can be predicted from qubit design or measured using an independent method. The parameters are extracted from a set of unstructured measurements. This allows us to use data even if it was produced for other purposes, for example to check wether the qubit couples to the flux line or not. In order to test our implemented procedure we measure the transition frequency $\omega_{01,i}^{(j)}$ of qubit i at random voltage configurations $\mathbf{V}^{(j)}$ in a region around $\mathbf{V} = \mathbf{0}$, where j enumerates the measurements. From this data set $\{(\omega_{01,i}^{(1)}, \mathbf{V}^{(1)}), (\omega_{01,i}^{(2)}, \mathbf{V}^{(2)}), \dots\}$ we determine the direction $\mathbf{n}_i = \mathbf{k}_i/|\mathbf{k}_i|$.

7.1 Determination of $\mathbf{k}_i$ via Fourier transform

When the measured data contains more than one period of $\omega_{01,i}(\mathbf{V})$, it is reasonable to use the Fourier transform to determine the vectors $\mathbf{k}_i$. In general we will get unstructured data and therefore we cannot use the discrete Fourier transform. Instead we use the transform

$$\mathcal{F}[\omega_{01,i}] = \frac{1}{N}\sum_{j=1}^{N} \omega_{01,i}^{(j)} e^{-2\pi i \mathbf{k}\cdot\mathbf{V}^{(j)}}. \tag{21}$$

Before we transform the experimental data, we subtract the mean $\langle \omega_{01,i}^{(j)} \rangle_j$ to eliminate the $\mathbf{k} = 0$ component in the Fourier space. Eliminating this component makes the later analysis simpler. The position of the maximum of $\mathcal{F}[\omega_{01,i}]$ is the vector $\mathbf{k}_i$.

From the Fourier transform we get, besides the direction of the vector $\mathbf{k}_i$, also its length $|\mathbf{k}_i|$. We can solve Equation 20 for the free parameters and get

$$E_{\mathrm{J},i}^{\max} \approx \frac{(\hbar\omega_{01,i}^{\max} + E_{\mathrm{C}})^2}{8E_{\mathrm{C}}} \tag{22}$$

$$\Phi_{\mathrm{env,i}} \approx (\mathbf{k}_i \mathbf{V}^{\max}) \bmod \Phi_0. \tag{23}$$

At the voltage $\mathbf{V}^{\max}$ we measured the largest transition frequency $\omega_{01,i}^{\max}$.

All measurements which were done during the thesis showed less than one period of $\omega_{01,i}$ and therefore the Fourier method was only tested on data from numerical simulation.

7.2 Determination of $\mathbf{n}_i$ via parabola fit

We need another procedure to find $\mathbf{k}_i$ if we have less than a period of $\omega_{01,i}$ in our measurement data. Then the Fourier transform is not relieable. In this case we approximate $\omega_i(\mathbf{V}) \approx -(\mathbf{a}_i \cdot \mathbf{V} + b_i)^2 + c_i$ in a first step. We fit this model to the data set $\{(\omega_{01,i}^{(1)}, \mathbf{V}^{(1)}), (\omega_{01,i}^{(2)}, \mathbf{V}^{(2)}), \dots\}$ to find $\mathbf{a}_i$, b_i and c_i. The direction $\mathbf{a}_i/|\mathbf{a}_i|$ is then, up to experimental and numerical errors, the direction $\mathbf{n}_i$ of the vector $\mathbf{k}_i$. The parameters b_i and c_i give the position of the maximum of the parabola. We are not interested in them, because later we fit the data to an accurate model and therefore get more accurate coordinates for the maximal transition frequency.

From the fit of the parabola to the data we do not get a reliable guess for the length $|\mathbf{k}_i|$ of the vector $\mathbf{k}_i$. Thus, we must use a different way to approximate the free parameters. For $E_{\mathrm{J},i}^{\max}$ we use the same guess value as for the Fourier transform method. The other guess values are

$$\Phi_{\mathrm{env,i}} \approx \frac{\Phi_0}{\pi} \arccos\left(\frac{(\hbar\omega_{01,i}^{\mathrm{zero}} + E_{\mathrm{C}})^2}{8E_{\mathrm{C}}E_{\mathrm{J}}^{\max}}\right) \tag{24}$$

$$|\mathbf{k}_i| \approx \frac{1}{\mathbf{V}_{\min}} \left[\frac{\Phi_0}{\pi} \arccos\left(\frac{(\hbar\omega_{01,i}^{\min} + E_{\mathrm{C}})^2}{8E_{\mathrm{C}}E_{\mathrm{J}}^{\max}}\right) - \Phi_{\mathrm{env,i}}\right] \tag{25}$$

where $\omega_{01,i}^{\mathrm{zero}}$ is the transition frequency that corresponds to the voltage setting $\mathbf{V}^{(j)}$ with the smallest magnitude $|\mathbf{V}^{(j)}|$ used in the experiment. The smallest measured transition frequency is $\omega_{01,i}^{\min}$ and $\mathbf{V}_{\min}$ the corresponding voltage.

7.3 Parameter Extraction

Once we have $\mathbf{n}_i$ we can project all vectors $\mathbf{V}^{(j)}$ onto its direction. This means we use the map

$$(\omega_{01,i}^{(j)}, \mathbf{V}^{(j)}) \to (\omega_{01,i}^{(j)}, \tilde{V}_i^{(j)}) \tag{26}$$

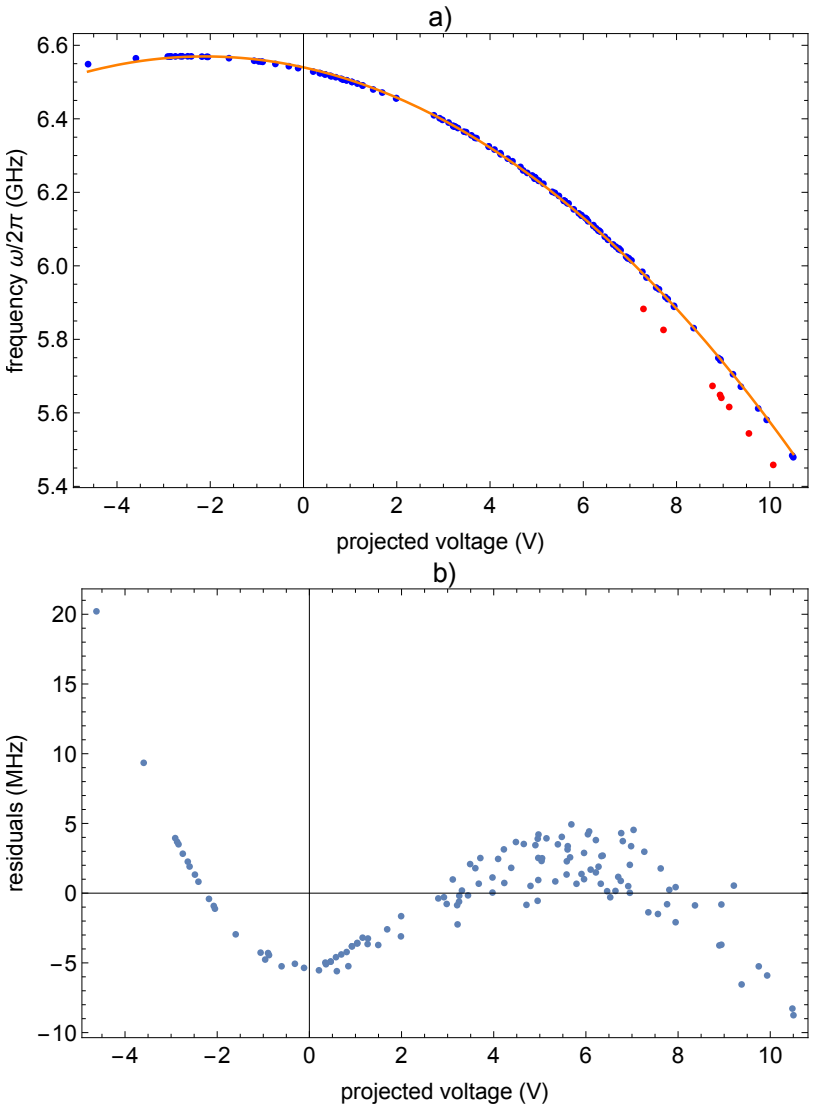

Figure 9: a) transition frequency $\omega_{01,1}$ of qubit 1 versus the voltage $\tilde{V}_1$. The blue dots represent the measured data and the solid orange line the fit. The red points correspond to $0 \leftrightarrow 2$ transitions. b) Residuals of the fit to the data in a).

with $\tilde{V}_i^{(j)} = \mathbf{V}^{(j)} \cdot \mathbf{n}_i$. We end up with a two dimensional data set $\{(\omega_{01,i}^{(1)}, \tilde{V}_i^{(1)}), (\omega_{01,i}^{(2)}, \tilde{V}_i^{(2)}), \dots\}$. We numerically minimize the residuals between this data and the exact model $\omega_{01,i}(\Phi_i)$ in terms of Mathieu functions. Finally, we can extract the values of the parameters $E_{\mathrm{J},i}^{\max}$, $\Phi_{\mathrm{env},i}$ and $|\mathbf{k}_i|$ from the fitted model.

In Figure 9a there are several systematic outliers. These outliers come from qubit spectroscopies where the qubit was driven with too high power. This led to excitations to the second energy level. Before the residuals were minimized, these outliers were filtered out by hand. The residuals

of the fit in Figure 9b lead to the conclusion that there is a model which describes the data more accurately. For example, our model of the qubit transition frequency does not include the coupling to the resonator and the possibility that the Josephson junctions have not exactly identical properties.

7.4 Voltages as Functions of the Qubit Transition Frequencies

For the purpose of setting the qubits to some frequency, we would like to know the function $\mathbf{V}(\boldsymbol{\omega}_{01})$ which calculates the voltages we have to apply to the coils in order to tune the qubits to the frequencies $\boldsymbol{\omega}_{01}$. We first calculate the Moore-Penrose pseudoinverse M^+ of the coupling matrix M. This pseudoinverse M^+ has the property that $MM^+ = \mathbb{1}$ if the rows of M are linearly independent. This condition should hold for the coupling matrix, because otherwise we could not tune the qubit frequencies independently. We want to find the inverse function $\boldsymbol{\Phi}(\boldsymbol{\omega}_{01})$ to the transition frequency. Because the transition freqeuncy is periodic in the magnetic flux, we need to choose a flux range on which the transition frequency is injective. It is sensible to choose this range close to the origin, therefore we choose the range $[0, \Phi_0/2]$. The relation $\boldsymbol{\Phi}(\boldsymbol{\omega}_{01})$ can approximately be obtained by inverting Equation 5. A more accurate but more costly way to find $\boldsymbol{\Phi}(\boldsymbol{\omega}_{01})$ is to solve $\boldsymbol{\omega}_{01}^{\text{exact}}(\boldsymbol{\Phi}) = \boldsymbol{\omega}_{01}$ for $\boldsymbol{\Phi}$, where $\boldsymbol{\omega}_{01}^{\text{exact}}(\boldsymbol{\Phi})$ is the exact solution in terms of Mathieu equations and $\boldsymbol{\omega}_{01}$ is the vector containing the transition frequencies we want to tune our qubits to.

7.5 Discussion

The described procedure allows us to determine the coupling of the qubit to the coils or flux lines. However, to determine the qubit-coil coupling, taking the spectrum of the qubit and the resonator must be done reasonably fast. In order to reliably determine the coupling of one qubit to one coil, we need a fixed number of measurements. To determine the coupling of n_q qubit to n_c coils we will need $\mathcal{O}(n_c n_q)$ measurements. One of the main goals of investigations on physical systems which can be used as qubits is to find a way to scale up the number of qubits. For higher number of qubits the determination of the qubit-coil coupling will take a considerable amount of time. Therefore, it is sensible to look for a method which needs as few measurements as possible. The advantage of the presented method is that it works with unstructured data. This means, we can use data from measurements which were performed for a different purpose to find the qubit-coil coupling.

8 Adaptive Bayesian Experimental Design

In general when we perform an experiment, we want to extract as much new information as possible per measurement we take. The adaptive Bayesian experimental design is a tool to perform experiments in a way such that the expected gain in our knowledge is maximized. This procedure does choose the measurement settings for the upcoming measurement based on the previously taken measurements. These settings are chosen such that they maximize an utility function. The utility function describes how usefull the outcome of the measurement will be in the sense of information that we gain about initially unknown parameters which describe the outcomes. In this chapter the algorithm described in [Granade et al., 2012] is summarized.

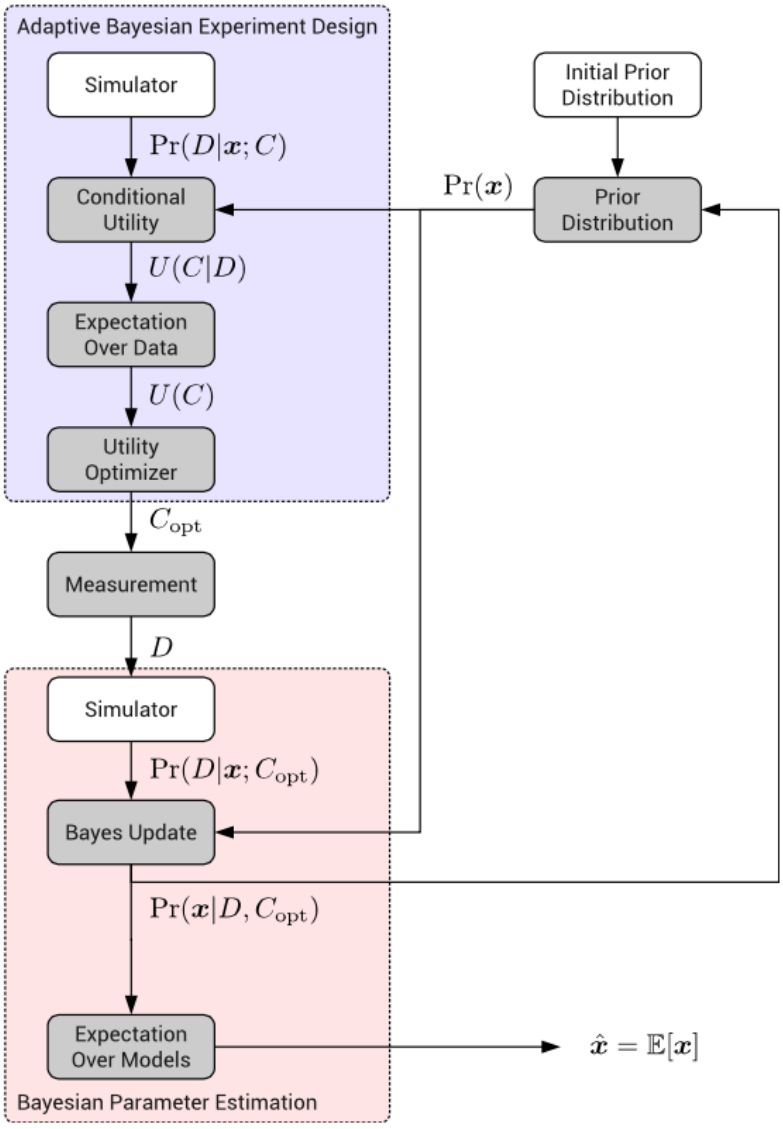

Figure 10: Overview of the algorithm. Adapted from [Granade et al., 2012].

Each experiment is described by an experiment configuration $\mathbf{c}$, a list of parameters $\mathbf{x}$ we want to determine and an outcome $\mathbf{d}$. In our case we have $\mathbf{x} = (\mathbf{E}_J^{\max}, \mathbf{\Phi}_{\text{env}}, \mathbf{k}_1, \mathbf{k}_2, \ldots, \mathbf{k}_{n_q})$, $\mathbf{d}_j = \boldsymbol{\omega}_{01}^{(j)}$ and $\mathbf{c}_j = \mathbf{V}^{(j)}$. Suppose we have perforemd already N experiments. Then we possess the sets $D_N = \{\mathbf{d}_1, \mathbf{d}_2 \ldots, \mathbf{d}_N\}$ and $C_N = \{\mathbf{c}_1, \mathbf{c}_2 \ldots, \mathbf{c}_N\}$ which contain all outcomes and all configurations of these experiments. Our knowledge about the physics behind the experiment is represented by a prior distribution $\Pr(\mathbf{x}|D_N; C_N)$ and a likelihood-function $\Pr(\mathbf{d}_{N+1}|\mathbf{x}; C_N, \mathbf{c}_{N+1}; D_N)$.

An overview of the algorithm is shown in Figure 10. The first step in the algorithm is to calculate the conditional utility $U(\mathbf{c}_{N+1}; \mathbf{d}_{N+1})$ and its expectation value over the possible outcomes of the

next experiment

$$U(\mathbf{c}_{N+1}) = \mathbb{E}_{\mathbf{d}_{N+1}|D_N;C_N,\mathbf{c}_{N+1}}[U(\mathbf{c}_{N+1};\mathbf{d}_{N+1})] \tag{27}$$

conditioned on the old data and all configurations. This expected utility $U(\mathbf{c}_{N+1})$ is then maximized to find the optimal configuration $\mathbf{c}_{\text{opt}}$ for the next experiment. New data $\mathbf{d}_{N+1}$ is generated by performing the experiment with the optimal configuration. Then the likelihood function and the prior distribution get updated with the new data and configurations, that means

$$\Pr(\mathbf{d}_{N+1}|\mathbf{x};C_{N+1};D_N) \to \Pr(\mathbf{d}_{N+2}|\mathbf{x};C_{N+2};D_{N+1}) \tag{28}$$

$$\Pr(\mathbf{x}|D_N;C_N) \to \Pr(\mathbf{x}|D_{N+1};C_{N+1}) \tag{29}$$

where $\mathbf{c}_{N+1} = \mathbf{c}_{\text{opt}}$. The same process is then iteratively repeated until some stop criterion is met, for example a certain number of iterations. Then the estimated parameters are calculated by taking the expectation value $\mathbb{E}_{\mathbf{x}|D_{N+1};C_{N+1}}[\mathbf{x}]$ with respect to the updated prior distribution.

The parameter space is usually continous and multidimensional. To avoid costly integrations over it, the approximation

$$\Pr(\mathbf{x}|D_N;C_N) \approx \sum_{k=1}^{n_x} w_k(D_N;C_N)\delta(\mathbf{x}-\mathbf{x}_k) \tag{30}$$

is used where n_x is the number of the so called particles $\mathbf{x}_k$. Following [Granade et al., 2012], we update the weights w_k by applying Bayes' rule

$$w_k(D_{N+1};C_{N+1}) \propto w_k(D_N;C_N)\Pr(D_{N+1}|\mathbf{x}_k;C_{N+1}). \tag{31}$$

We normalize the w_k s.t. $\sum_k w_k = 1$. The utility function is the information gain

$$\begin{aligned} U(\mathbf{c}_{N+1};\mathbf{d}_{N+1}) &= \mathbb{E}_{\mathbf{x}|D_{N+1};C_{N+1}}[\log\Pr(\mathbf{x}|D_{N+1};C_{N+1})] \\ &\approx \sum_{k=1}^{n_x} w_k \log\Pr(\mathbf{x}_k|D_{N+1};C_{N+1}) \\ &= \sum_k w_k \log\left(\frac{\Pr(\mathbf{d}_{N+1}|\mathbf{x}_k;D_N;C_{N+1})\Pr(\mathbf{x}_k|D_N;C_{N+1})}{\Pr(\mathbf{d}_{N+1}|D_N;C_{N+1})}\right) \end{aligned} \tag{32}$$

In [Lindley, 1956] this choice of utility function is motivated rigorously. To get an intuition why this utility function is reasonable, we look at a simple case. Consider we have m different values for $\mathbf{x}$ and we have taken no measurements. Further we should not have prior knowledge, meaning $\Pr(\mathbf{x})$ is uniform. If there is someone who knows $\mathbf{x}$ and we want to ask for the value of it, we have to ask $\log_2 m$ questions which can be answered with 'yes' or 'no'. The information gain utility function is in this case $U = \sum_{\mathbf{x}} \Pr(\mathbf{x})\log\Pr(\mathbf{x}) = -\log m$, which is proportional to the negative of the number of questions we have to ask. This means the higher the utility, the less questions we have to ask to find $\mathbf{x}$. We can go a step further and assume we performed a measurement which told us that only half of the m different values for $\mathbf{x}$ are possible, but still with uniform probabilities. This new knowledge will reduce the number of questions we have to ask by one and the utility increases accordingly. Therefore, the information gain utility can be used as a measure for the information we possess about the parameter $\mathbf{x}$. However, the utility function is not uniquely determined, there are several measures for the usefulness of the experimental setting. Another possible choice is the negative variance [Granade et al., 2012].

Before calculating the expected utility, we notice that having an additional setting c_{N+1} does not change our knowledge about the parameters, i.e. $\Pr(\mathbf{x}_k|D_N;C_{N+1}) = \Pr(\mathbf{x}_k|D_N;C_N)$. Terms proportional to $\log\Pr(\mathbf{x}_k|D_N;C_{N+1})$ can be neglected in the expected utility as we are only interested in terms depending on c_{N+1}. The utility is

$$\begin{aligned} U(\mathbf{c}_{N+1}) &= \sum_{k=1}^{n_x} w_k \mathbb{E}_{\mathbf{d}_{N+1}|D_N;C_{N+1}}[\log\Pr(\mathbf{d}_{N+1}|\mathbf{x}_k;D_N;C_{N+1})] \\ &\quad - \mathbb{E}_{\mathbf{d}_{N+1}|D_N;C_{N+1}}[\log\Pr(\mathbf{d}_{N+1}|D_N;C_{N+1})] \\ &= H_{\mathbf{d}_{N+1}|D_N;C_{N+1}}[\Pr(\mathbf{d}_{N+1}|D_N;C_{N+1})] \\ &\quad - \sum_{k=1}^{n_x} w_k H_{\mathbf{d}_{N+1}|D_N;C_{N+1}}[\Pr(\mathbf{d}_{N+1}|\mathbf{x}_k;D_N;C_{N+1})] \end{aligned} \tag{33}$$

where H denotes the entropy.

In our experiment the initial prior distribution is a product distribution $\prod_i \Pr(E_{J,i}^{\max})\Pr(\mathbf{k}_i)\Pr(\Phi_{\text{env},i})$. The distribution of $E_{J,i}^{\max}$ is a normal distribution around an estimated mean value. The random variable $\Phi_{\text{env},i}$ is also normally distributed with mean at zero. The j-th component of the i-th vector $k_{i,j}$ is normally distributed around zero if i is not equal to j and otherwise it is uniformly distibuted. The likelihood function takes the form $\Pr(\boldsymbol{\omega}_{01}|\mathbf{E}_J^{\max},\mathbf{k}_1,\ldots,\mathbf{k}_{n_q},\boldsymbol{\Phi}_{\text{env}};\mathbf{V}) = \prod_{i=1}^{n_q}\Pr(\omega_{01,i}|\mathbf{E}_{J,i}^{\max},\mathbf{k}_i,\Phi_{\text{env,i}};\mathbf{V})$. The factors are normal distributed $\Pr(\omega_{01,i}|\mathbf{E}_{J,i}^{\max},\mathbf{k}_i,\Phi_{\text{env,i}};\mathbf{V}) \sim \mathcal{N}(\mu_i,\sigma_i)$ with the mean values $\mu_i = \omega_{01,i}(\mathbf{V})$ and a narrow widths σ_i due to experimental errors. The approximation described in Equation 30 is done by sampling the set of Josephson energies, flux offsets and coupling vectors. This means that the mean $\mu_{i,k}$ gets another index k to enumerate the particles $\mathbf{x}_k$ in the parameter space.

8.1 Discussion

Having all the initial distributions, we could apply the algorithm. However, we have a continuous space of possible measurement outcomes $\mathbf{d}$. This fact comes into play when we want to compute the expected utility. The first term in Equation 33 takes the form

$$\begin{aligned} &H_{\boldsymbol{\omega}^{(N+1)}|D_N;C_{N+1}}[\Pr(\boldsymbol{\omega}^{(N+1)}|D_N;C_{N+1})] = \\ &\int \mathrm{d}\boldsymbol{\omega}_{01} \sum_{k=0}^{n_x} w_k \prod_{i=1}^{n_q} f(\omega_{01,i}|\mu_{i,k},\sigma_i) \log\left[\sum_{l=0}^{n_x} w_l \prod_{j=1}^{n_q} f(\omega_{01,j}|\mu_{j,l},\sigma_j)\right] \end{aligned} \tag{34}$$

where $f(\omega_{01,i}|\mu_{i,k},\sigma_i)$ is the probability density function of $\Pr(\omega_{01,i}|\mathbf{E}_{J,i}^{\max},\mathbf{k}_i,\Phi_{\text{env,i}};\mathbf{V})$. This integral is not analytically solvable in contrast to the other terms in Equation 33. One approach to solve it is to use Monte Carlo integration. This allows us to replace the integration by a summation. When we consider n_x particles in the parameter space and n_d particles in the space of the measurement outcomes, we have to perform $n_x \cdot n_d$ operations to evaluate the expected utility function at one specific configuration $\mathbf{c}$. For a reasonable precision we need particle numbers of the order of thousands in each space and therefore we need millions of operations to evaluate the utility function once. We maximize the utility function to find the optimal configuration. This means we have to evalutate the utility function serveral times. The implementation of the utility function for

our experiment can be evaluated in tenths of seconds. Assuming that we get a reasonably good configuration by evaluating only of the order of ten times, we can find the configuration on a time scale of seconds. One should notice here that taking a nonoptimal configuration for the experiment means that we have to measure at more different points to get the same accuracy for the estimated parameter. Therefore there is a tradeoff between time used for computation and time used for taking measurements.

For our experiment the utility function is still under development. We tried to approximate the integrand of the utility function such that we can analytically solve the integral, but we did not succeed. Then we implemented the Monte Carlo integration over the space of measurement outcomes. This led to an utility function which does not converge as a function of the Monte Carlo particles n_d.

In other experiments the adaptive Bayesian experiment design can be useful, especially when we have only a few different possible measurement outcomes. This is for example the case if we would like to find the decoherence time and therefore read out the qubit states at different times. In this case we have only two possible measurement outcomes and therefore the evaluation of the expected utility only takes time of the order of $2n_x$.

This is the first study of the adaptive Bayesian experimental design in the Quantum Device Lab. However, there exist various experimental techniques for different tasks related to quantum information processing based on the Bayesian approach. These techniques are interesting, as they try to minimize the resources needed to perform certain tasks. A selection of potentially usefull techniques for quantum information processing are accelerated randomized benchmarking [Granade and Ferrie, 2015], adaptive quantum tomography of two-qubit states [Struchalin et al., 2016] and quantum model averaging [Ferrie, 2014].

9 Conclusion and Outlook

Previous to this work the Software suite was able to perform qubit and resonator spectroscopies. However, the determination of the transition frequency and the resonant frequency had to be done by hand. Now, the software is able to find them, provided the user tells the program a frequency range which contains these frequencies. In addition, the software was extended with functionalities which allow to automatically determine the coupling of the qubit transition frequency to a coil or flux line via magnetic flux. The software can now use unstructured voltage configurations to find the parameters describing the coupling.

A Bayesian approach to experimental design was studied with the aim to minimize the time needed to determine the qubit-coil coupling. The core features of this design were implemented and tested. We concluded that the implementation is not yet ready to be used for qubit characterization and needs further improvement and testing. However, the study of this approach revealed some techniques which might be useful for other tasks related to quantum computation.

In a future work on the software, one could implement the possiblity to determine the qubit-coil coupling 'on the fly'. For this purpose we can imagine an experiment in which we would like to tune the qubit transition frequency to some given value. We start by measuring our current qubit

transition frequency. Then we change the voltages on the coils by a small amount and measure again. Using these two measurements we do a linear approximation of the qubit-coil coupling. This approximation gives us an estimate of how we have to tune the voltages to get closer to our desired transition frequency. This procedure of measuring and approximating is repeated until we are in a certain region around our desired transition frequency. After the iterative tuneup was performed, we can use the collected data to find the qubit-coil coupling. The ability of the software to use unstructured voltage configurations paves the way for adding such functionality.

A procedure which is often used, especially during the characterization of the processor sample, is qubit spectroscopy. Therefore it is reasonable to optimize this procedure. A way to reduce time consumption is to guess the qubit transition frequency based on the already collected data. For example if we know the qubit transition frequency at a specific voltage configuration, then we can assume that a small change in voltage leads to a small change in frequency. This means for small voltage changes we have to look for the qubits transition frequency only in a small region around the transition frequency for the previous voltage configuration. This would allow us to perform qubit spectroscopy faster because we can decrease the frequency range we sweep over during spectoscopy. The same could be done for the resonator spectroscopy.

10 Acknowledgements

I would like to thank Prof. Dr. Andreas Wallraff for giving me the opportunity to conduct my semester thesis in The Quantum Device Lab. My special thanks go to my supervisor Johannes Heinsoo. He could always give me useful advice when I asked for and discussing with him often led to new insights, at least for me, into the experiments and the physics behind it. He always motivated the tasks I did during my thesis in a clear way. I would also thank Simon Storz who conducted the master thesis during my time at the QuDev. He supported me with his knowledge about the Software suite and he took qubit and resonator spectroscopy measurements for my work. Last but not least, I would like to thank the QuDev team for giving me a good time while I was working on this thesis.

References

[Baur, 2012] Baur, M. (2012). *Realizing quantum gates and algorithms with three superconducting qubits*. PhD thesis, ETH Zurich.

[Benhelm et al., 2008] Benhelm, J., Kirchmair, G., Roos, C. F., and Blatt, R. (2008). Experimental quantum-information processing with ca-43(+) ions. *Phys. Rev. A*, 77(6).

[Blais et al., 2004] Blais, A., Huang, R.-S., Wallraff, A., Girvin, S. M., and Schoelkopf, R. J. (2004). Cavity quantum electrodynamics for superconducting electrical circuits: An architecture for quantum computation. *Phys. Rev. A*, 69(6):062320–14.

[Bouchiat et al., 1998] Bouchiat, V., Vion, D., Joyez, P., Esteve, D., and Devoret, M. H. (1998). Quantum coherence with a single Cooper pair. *Phys. Scr.*, T76:165–170.

[Bremner et al., 2002] Bremner, M. J., Dawson, C. M., Dodd, J. L., Gilchrist, A., Harrow, A. W., Mortimer, D., Nielsen, M. A., and Osborne, T. J. (2002). Practical scheme for quantum computation with any two-qubit entangling gate. *Phys. Rev. Lett.*, 89:247902.

[Chen et al., 2012] Chen, Y., Sank, D., O'Malley, P., White, T., Barends, R., Chiaro, B., Kelly, J., Lucero, E., Mariantoni, M., Megrant, A., Neill, C., Vainsencher, A., Wenner, J., Yin, Y., Cleland, A. N., and Martinis, J. M. (2012). Multiplexed dispersive readout of superconducting phase qubits. *arXiv:1209.1781*.

[Ciorciaro, 2015] Ciorciaro, L. (2015). Automatic single qubit routines. Bachelor thesis, ETH Zurich.

[Clarke and Wilhelm, 2008] Clarke, J. and Wilhelm, F. K. (2008). Superconducting quantum bits. *Nature*, 453(7198):1031–1042.

[Cottet et al., 2002] Cottet, A., Vion, D., Aassime, A., Joyez, P., Esteve, D., and Devoret, M. H. (2002). Implementation of a combined charge-phase quantum bit in a superconducting circuit. *Physica C*, 367(1-4):197–203.

[Deutsch and Jozsa, 1992] Deutsch, D. and Jozsa, R. (1992). Rapid solution of problems by quantum computation. *Proceedings: Mathematical and Physical Sciences*, 439(1907):553–558.

[DiCarlo et al., 2009] DiCarlo, L., Chow, J. M., Gambetta, J. M., Bishop, L. S., Johnson, B. R., Schuster, D. I., Majer, J., Blais, A., Frunzio, L., Girvin, S. M., and Schoelkopf, R. J. (2009). Demonstration of two-qubit algorithms with a superconducting quantum processor. *Nature*, 460(7252):240–244.

[DiVincenzo, 2000] DiVincenzo, D. P. (2000). The physical implementation of quantum computation. *Fortschritte der Physik*, 48(9-11):771–783.

[Ferrie, 2014] Ferrie, C. (2014). Quantum model averaging. *New Journal of Physics*, 16(9):093035.

[Gershenfeld and Chuang, 1997] Gershenfeld, N. and Chuang, I. (1997). Bulk spin resonance quantum computation. *Science*, 275:350–356.

[Granade et al., 2012] Granade, C., Ferrie, C., Wiebe, N., and Cory, D. (2012). Robust online hamiltonian learning. *New Journal of Physics*, 14.

[Granade and Ferrie, 2015] Granade, C. and Ferrie, C., C. D. (2015). Accelerated randomized benchmarking. *New Journal of Physics*, 17.

[Grover, 1996] Grover, L. K. (1996). A fast quantum mechanical algorithm for database search. In *Proceedings of the twenty-eighth annual ACM symposium on Theory of computing*, pages 212–219, Philadelphia, Pennsylvania, United States. ACM.

[Heinsoo, 2013] Heinsoo, J. (2013). Automatic multi-qubit gate calibration. Semester thesis, ETH Zurich.

[Josephson, 1962] Josephson, B. D. (1962). Possible new effects in superconductive tunnelling. *Physics Letters*, 1(7):251–253.

[Knill et al., 2001] Knill, E., Laflamme, R., and Milburn, G. J. (2001). A scheme for efficient quantum computation with linear optics. *Nature*, 409(6816):46–52.

[Koch et al., 2007] Koch, J., Yu, T. M., Gambetta, J., Houck, A. A., Schuster, D. I., Majer, J., Blais, A., Devoret, M. H., Girvin, S. M., and Schoelkopf, R. J. (2007). Charge-insensitive qubit design derived from the Cooper pair box. *Phys. Rev. A*, 76(4):042319.

[Lindley, 1956] Lindley, D. V. (1956). On a measure of the information provided by an experiment. *Ann. Math. Stat*, 27:986.

[Nakamura et al., 1997] Nakamura, Y., Chen, C. D., and Tsai, J. S. (1997). Spectroscopy of energy-level splitting between two macroscopic quantum states of charge coherently superposed by josephson coupling. *Phys. Rev. Lett.*, 79:2328–2331.

[Neumann et al., 2010] Neumann, P., Kolesov, R., Naydenov, B., Beck, J., Rempp, F., Steiner, M., Jacques, V., Balasubramanian, G., Markham, M. L., Twitchen, D. J., Pezzagna, S., Meijer, J., Twamley, J., Jelezko, F., and Wrachtrup, J. (2010). Quantum register based on coupled electron spins in a room-temperature solid. *Nat. Phys.*, 6(4):249–253.

[Schaller, 1997] Schaller, R. R. (1997). Moore's law: Past present and future. *IEEE Spectrum*, page 53.

[Shor, 1997] Shor, P. W. (1997). Polynomial-time algorithms for prime factorization and discrete logarithms on a quantum computer. *SIAM Journal on Scientific and Statistical Computing*, 26:1484.

[Storz, 2016] Storz, S. (2016). In preparation. Master's thesis, ETH Zurich.

[Struchalin et al., 2016] Struchalin, G. I., Pogorelov, I. A., Straupe, S. S., Kravtsov, K. S., Radchenko, I. V., and Kulik, S. P. (2016). Experimental adaptive quantum tomography of two-qubit states. *Phys. Rev. A*, 93:012103.

[Wallraff et al., 2004] Wallraff, A., Schuster, D. I., Blais, A., Frunzio, L., Huang, R.-S., Majer, J., Kumar, S., Girvin, S. M., and Schoelkopf, R. J. (2004). Strong coupling of a single photon to a superconducting qubit using circuit quantum electrodynamics. *Nature*, 431:162–167.

[Zimmerman, 1977] Zimmerman, J. E. (1977). Squid instruments and shielding for low-level magnetic measurements. *J. Appl. Phys.*, 48.

ETH

Eidgenössische Technische Hochschule Zürich
Swiss Federal Institute of Technology Zurich

Declaration of originality

The signed declaration of originality is a component of every semester paper, Bachelor's thesis, Master's thesis and any other degree paper undertaken during the course of studies, including the respective electronic versions.

Lecturers may also require a declaration of originality for other written papers compiled for their courses.

I hereby confirm that I am the sole author of the written work here enclosed and that I have compiled it in my own words. Parts excepted are corrections of form and content by the supervisor.

Title of work (in block letters):

Automatic Analysis of Transmon Qubit Spectroscopy and Coil Coupling Measurements

Authored by (in block letters):

For papers written by groups the names of all authors are required.

Name(s):	**First name(s):**
Grünenfelder	Fadri

With my signature I confirm that

- I have committed none of the forms of plagiarism described in the 'Citation etiquette' information sheet.
- I have documented all methods, data and processes truthfully.
- I have not manipulated any data.
- I have mentioned all persons who were significant facilitators of the work.

I am aware that the work may be screened electronically for plagiarism.

Place, date	**Signature(s)**
Alvaneu Dorf, 16.09.2018	F. Gf

For papers written by groups the names of all authors are required. Their signatures collectively guarantee the entire content of the written paper.